Applied Catalysis B: Environmental 328 (2023) 122519

Contents lists available at ScienceDirect

Applied Catalysis B: Environmental

journal homepage: www.elsevier.com/locate/apcatb

Constructing Ru particles decorated Co_3B-CoP heterostructures as a highly active and reusable catalyst for H_2 generation by catalyzing $NaBH_4$ hydrolysis

Shuqing Zhou [a], Lianrui Cheng [a], Yi Huang [a], Yi Liu [a], Luyan Shi [a], Tayirjan Taylor Isimjan [b], Xiulin Yang [a,*]

[a] Guangxi Key Laboratory of Low Carbon Energy Materials, School of Chemistry and Pharmaceutical Sciences, Guangxi Normal University, Guilin 541004, China
[b] Saudi Arabia Basic Industries Corporation (SABIC) at King Abdullah University of Science and Technology (KAUST), Thuwal 23955-6900, Saudi Arabia

ARTICLE INFO

Keywords:
Co_3B-CoP
Electronic interaction
$NaBH_4$ hydrolysis
Hydrogen generation
Catalytic mechanism

ABSTRACT

Constructing an efficient and reusable catalyst for catalyzing $NaBH_4$ hydrolysis for H_2 production is of vital significance. Herein, the Ru particles decorated Co_3B-CoP heterostructures are obtained by chemical reduction and gas-phase phosphating treatment. The strong electronic interaction and abundant heterojunctions between the Co_3B-CoP substrate and Ru particles have been elucidated. The optimal $Ru_{0.063}/Co_3B$-CoP catalyst exhibits a fast hydrogen generation rate (8875.8 mL min^{-1} g_{cat}^{-1}) and a high turnover frequency (636.0 min^{-1}) at 25 °C, superior to most ever reported catalysts. The excellent $NaBH_4$ hydrolysis performance can be attributed to the lower activation energy (47.6 kJ mol^{-1}) and the synergy between Co_3B-CoP substrate and Ru particles. Density functional theory calculations show that electrons penetrate into Ru particles from Co_3B-CoP substrate, in which the electron-rich Ru particles can selectively adsorb BH_4^- ions, while the electron-deficient Co_3B-CoP facilitates the capture of H_2O molecules, thereby synergistically promote the catalyzing $NaBH_4$ hydrolysis to produce H_2.

1. Introduction

With negative environmental issues and severe energy deficiency owing to the ongoing depletion of traditional fossil fuels, it is urging to seek clean and sustainable alternative energy [1]. Hydrogen (H_2) has been deemed the most suitable energy carrier to replace fossil fuels due to its high energy density and environmental protection characteristics [2,3]. However, the production and storage of H_2 remain a great challenge for the widespread use and industrialization of hydrogen fuel cell devices [4]. Therefore, finding efficient, sustainable, and reusable hydrogen storage sources is imperative to realize safe production and storage of hydrogen [5].

Metal hydrides have received widespread attention owing to their advantage of high hydrogen storage capacity, non-toxicity and mild reaction conditions. Nowadays, the commonly used metal hydrogen storage materials include MgH_2 [6], $LiAlH_4$ [7], $NaBH_4$ [8], etc. Among them, $NaBH_4$ has a high hydrogen storage density (10.6 wt%), as well as stably stored in an alkaline solution, which is favorable to catalyze the hydrolysis of $NaBH_4$ to release H_2 in a controllable manner [9,10]. Most notably, Zhu et al. successfully used a very simple, lightweight and effective ball milling technology to regenerate the by-products of $NaBH_4$, realizing the reusability of $NaBH_4$ [11]. Benefiting from these feasible regeneration technologies, the application of H_2 generation by $NaBH_4$ hydrolysis has a broader industrialization prospect. Unfortunately, the self-hydrolysis of $NaBH_4$ suffers from sluggish kinetics, and is far from satisfying people's needs [12]. Driven by the requirements of rapid industrialization, it is necessary to add suitable catalysts to increase the rate of $NaBH_4$ hydrolysis to release hydrogen [13,14]. Generally, in order to inhibit the self-hydrolysis of $NaBH_4$, NaOH is added as a stabilizer to achieve the purpose of producing hydrogen on demand. The ideal hydrolysis reaction equation of $NaBH_4$ is as follows [15]:

$$NaBH_4 + (2+x)H_2O \xrightarrow{\text{Catalyst}} NaBO_2 \cdot xH_2O + 4H_2 \quad (1)$$

Many recent reports have proved that noble metal-based catalysts are remarkable catalysts for the hydrolysis of sodium borohydride, such as RuP_3-CoP [16], Ru-Co/CNTs [17], Ru-Fe/GO [18], Rh/Co_3O_4 [19], Pt/CeO_2 $-Co_7Ni_2O_x$ [20], etc. Nevertheless, the relatively high cost and

* Corresponding author.
E-mail address: xlyang@gxnu.edu.cn (X. Yang).

https://doi.org/10.1016/j.apcatb.2023.122519
Received 19 November 2022; Received in revised form 14 January 2023; Accepted 22 February 2023
Available online 23 February 2023

scarcity of noble metals seriously affect their widespread industrial application. Suitable support can not only regulate the content of noble metals, but also enhance the catalytic activity through the synergistic effect of noble metals and support [21,22]. Recently, many cobalt-based catalysts have exhibited great potential activity for hydrogen production by $NaBH_4$ hydrolysis [23,24].

Herein, we have successfully synthesized Ru clusters modified Co_3B-CoP heterostructures through wet chemical reduction and gas-phase phosphating under N_2. Systematic characterization techniques have been applied to explore the crystallinity, microstructure, porosity, and chemical state of different components. Density functional theory (DFT) calculations show that the $Ru_{0.063}/Co_3B$-CoP catalyst has a lower chemical potential for hydrogen hydrolysis. Performance tests demonstrate that $Ru_{0.063}/Co_3B$-CoP catalyst exhibits high hydrogen generation rate (HGR, 8875.8 mL_{H2} min^{-1} g_{cat}^{-1}) and turnover frequency (TOF, 636.0 mol min^{-1} mol_{Ru}^{-1}) values, as well as a low activation energy (47.6 kJ mol^{-1}). This outstanding catalytic performance can be attributed to the strong electronic interaction between Co_3B-CoP substrate and Ru particles, which facilitates to the capture and cleavage of H_2O molecules and BH_4^- ions, respectively, thereby accelerating the catalytic hydrolysis of $NaBH_4$ for H_2 production.

2. Experimental section

2.1. Materials

Cobalt(II) chloride hexahydrate ($CoCl_2{\cdot}6\ H_2O$), Sodium borohydride ($NaBH_4$), Sodium hydroxide (NaOH), Sodium hypophosphite ($NaH_2PO_2{\cdot}H_2O$), Cobalt(II) nitrate hexahydrate ($Co(NO_3)_2{\cdot}6\ H_2O$), Hexamethylenetetramine ($C_6H_{12}N_4$), and Ruthenium(III) chloride hydrate ($RuCl_3{\cdot}xH_2O$). All chemicals are analytically pure and can be used without further purification. The aqueous solutions in this work were prepared from ultrapure water with a resistivity of 18.2 MΩ·cm, obtained from a UPTA-20 water purification system (China Shanghai Lichen Bangxi Instrument Technology Co., Ltd.).

2.2. Synthesis of Co_3B

The synthetic process of Co_3B referred to the reported literature with some modifications [25]. Typically, 30.0 mL of $CoCl_2$ solution (0.5 M) was placed in ice water bath and stirred magnetically. Subsequently, Ar was rinsed in the solution for 30 min, and then 10.0 mL of $NaBH_4$ solution (1.0 M) was added dropwise to the solution, followed by stirring for another 30 min. After centrifugation and washing with water several times, as well as vacuum drying at 60 °C for 12 h, a black Co_3B powder was obtained.

2.3. Synthesis of Co_3B-CoP

The Co_3B-CoP heterostructure was synthesized with Co_3B and $NaH_2PO_2{\cdot}H_2O$ as precursors. Specifically, 1.0 g of $NaH_2PO_2{\cdot}H_2O$ was on the upstream, and 0.08 g of Co_3B were place in the downstream. The tube furnace was heated to 350 °C (5 °C min^{-1}) in N_2 atmosphere and maintained for 2 h. After natural cooling, the received precursor was denoted as Co_3B-CoP.

2.4. Synthesis of Ru/Co_3B-CoP

In a typical procedure, 30.0 mg as-synthesized Co_3B-CoP were ultrasonically dispersed in 20.0 mL deionized water containing 9.0 mg (or 3.0, 6.0, 12.0 and 15.0 mg) $RuCl_3$, and allowed to react at room temperature for 4 h with stirring. Subsequently, 10.0 mL of 0.08 M $NaBH_4$ solution was added dropwise to above mixture and reacted for another 30 min. The product was collected by centrifugation, washed several times with abundant H_2O, and then vacuum dried at 60 °C for 12 h. Commercial $RuCl_3{\cdot}xH_2O$ is used to prepare a specific concentration solution and then disperse it with a certain amount of substrate weighed accurately. An excessive amount of reducing agent is used to ensure the complete reaction of Ru ions. The mass content of Ru determined by ICP-AES measurement was 6.3 wt%, so the product was labelled as $Ru_{0.063}/Co_3B$-CoP, where the subscript 0.063 represented the mass percentage of Ru. Repeated experiments ensure the reproducibility of the catalyst. For comparison, $Ru_{0.02}/Co_3B$-CoP, $Ru_{0.047}/Co_3B$-CoP, $Ru_{0.089}/Co_3B$-CoP and $Ru_{0.113}/Co_3B$-CoP were also prepared by the same approach as that of $Ru_{0.063}/Co_3B$-CoP.

2.5. Synthesis of Ru/CoP

Typically, 0.58 g $Co(NO_3)_2$ and 0.56 g hexamethylenetetramine were dissolved in 15.0 mL deionized water with stirring for 30 min to obtain a uniform solution. Next, the mixture was transferred to a 50 mL Teflon-lined autoclave and raised to 100 °C for 10 h. After natural cooling, the product was collected by centrifugation, washed and then freeze-dried overnight. As a comparison, $Co(OH)_2$ was first phosphated to CoP using vapor-phase phosphating, and then Ru precursor was deposited on CoP surface (Ru/CoP) by chemical reduction as described above.

2.6. Catalytic measurements

The hydrolysis rate, activation energy and reusability of $NaBH_4$ were obtained to evaluate the performance of catalysts through following methods. Generally, 50 mL of 150 mM $NaBH_4$ + 0.4 wt% NaOH solution was injected into a 100 mL three-necked round-bottom flask, which was then placed in a water bath at 298 K and stirred for 30 min until the temperature remained constant. Subsequently, 10.0 mg of the catalyst was added to the above solution and stirred magnetically. The generated H_2 was collected by the drainage approach, which connected to a computer to record the change of water quality instantly. For recyclability testing of catalysts, we continued to replace the completely decomposed $NaBH_4$ solution with fresh one for five consecutive cycles at 298 K. After each stability test, the catalytic material was centrifuged, washed and vacuum dried, as well as weighed the catalytic material. All experiments were repeated three times to ensure reliable results. For the evaluation of the activation energy of catalysts, the reaction temperature was controlled from 298 K to 318 K for the catalytic hydrolysis of $NaBH_4$, and then the activation energy was calculated by the Arrhenius formula.

3. Results and discussion

3.1. Synthesis strategy and microstructure analysis

The Ru/Co_3B-CoP catalyst is constructed by the following multistep fabrication procedures (Fig. 1a). Firstly, the magnetic Co_3B is synthesized in an ice bath under Ar protection. Among them, the strong reducing agent $NaBH_4$ makes the preparation process of Co_3B extremely rapid and violent, while the low temperature environment can weaken the reaction and reduce the aggregation of Co_3B particles (Fig. 1b). Subsequently, using NaH_2PO_2 as the phosphorus source, Co_3B is phosphatized to Co_3B-CoP heterostructure under N_2 atmosphere. Fig. 1c presents that Co_3B-CoP retains its initial shape with slightly larger size and smoother surface, which caused by the 2 h aging process at 350 °C. Since the reduction potential of $NaBH_4$ (1.24 V) is much higher than that of Ru^{3+}/Ru (0.75 V), Ru ions are reduced to form the target catalyst when the two precursors are initially contacted; thereby, the Ru precursor is successfully reduced and anchored on the surface of the Co_3B-CoP composite before behaving as the hydrolysis catalyst. The as-prepared $Ru_{0.063}/Co_3B$-CoP hybrid composite still maintains a particulate structure with almost no visible changes (Fig. 1d).

Transmission electron microscopy (TEM) is further performed to analyze the microstructure of $Ru_{0.063}/Co_3B$-CoP. The Co_3B, Co_3B-CoP,

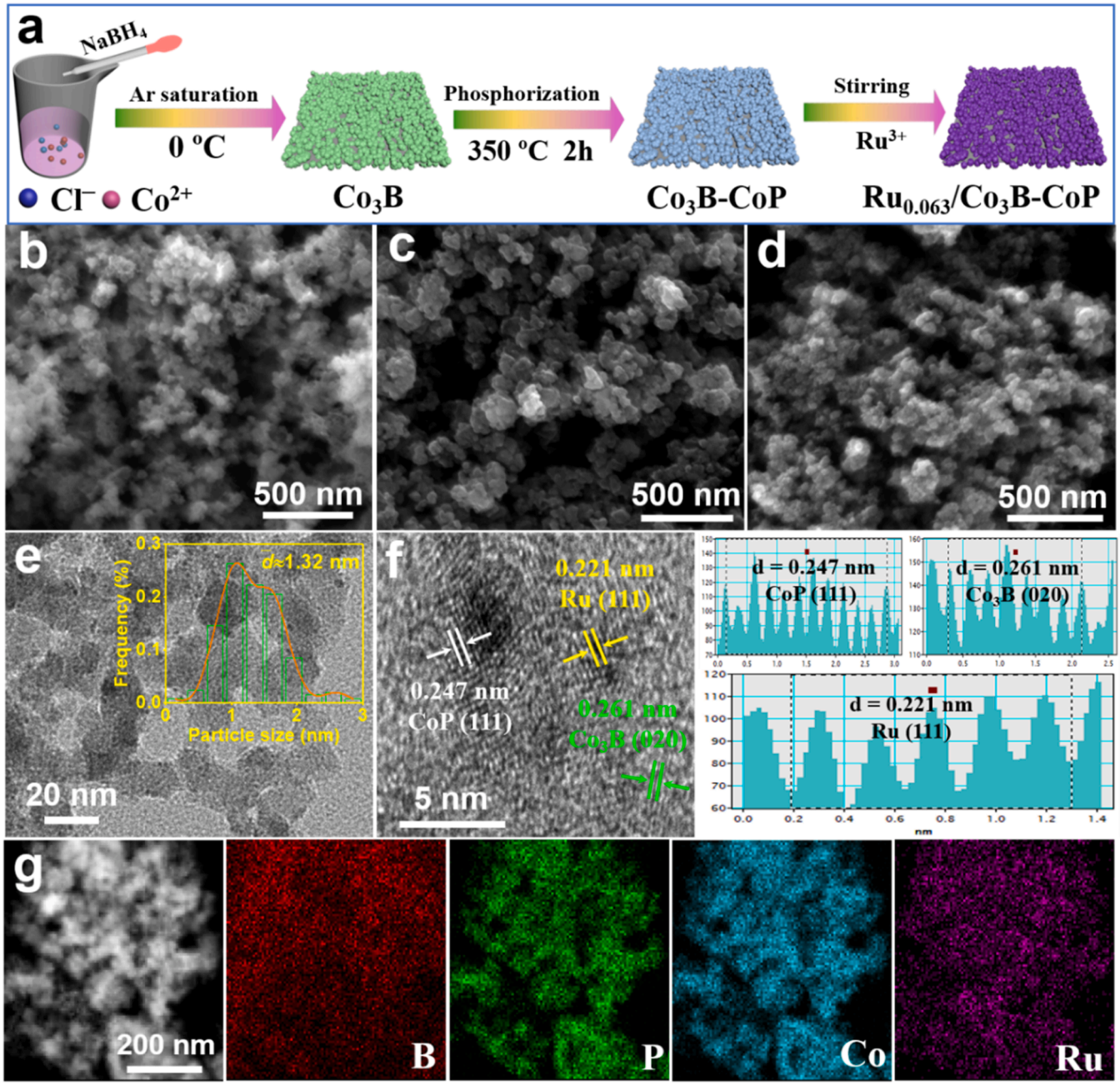

Fig. 1. (a) Schematic diagram of $Ru_{0.063}/Co_3B$-CoP synthesis. SEM images of (b) Co_3B, (c) Co_3B-CoP, and (d) $Ru_{0.063}/Co_3B$-CoP. (e) TEM image with inset particle size distribution of Ru particles, and (f) HRTEM image of $Ru_{0.063}/Co_3B$-CoP. (g) HAADF-TEM image and elemental mappings of $Ru_{0.063}/Co_3B$-CoP (B, P, Co and Ru).

and $Ru_{0.063}/Co_3B$-CoP catalysts are nanoparticles with a 50–200 nm grain size (Fig. 1b, c, and d). As shown in Fig. 1e, the Ru particles are dispersed uniformly throughout the catalyst, with an average cluster size of 1.32 nm. While the average sizes of Ru particles for $Ru_{0.063}$/CoP and $Ru_{0.063}/Co_3B$ catalysts are 1.84 and 1.95 nm, respectively (Fig. S1), indicating that the Co_3B-CoP heterostructure has a positive effect on the dispersion of Ru particles [26]. Meanwhile, the high-resolution TEM images revealed that the Ru on the surface is composed of Ru (111, 0.221 nm) [27]. Moreover, the crystal orientation and the lattice spacing of Co_3B (020, 0.261 nm) and CoP (111, 0.247 nm) are also detected (Fig. 1f) [28,29]. In addition, the high-annular dark-field scanning TEM (HAADF-STEM) image and corresponding element mappings (Fig. 1g) demonstrate the uniform distribution of B, P, Co, and Ru throughout the composite [30].

3.2. Crystal structure analysis

The phase composition and crystal structure of the composite was elucidated by X-ray diffraction (XRD). As displayed in Fig. 2a, the diffraction peaks, which concentrated between 30 and 60 ° are indexed to the standard diffraction peaks (JCPDS: 12–0443) of orthorhombic Co_3B. [31]. After the phosphating treatment, in addition to the diffraction peaks of Co_3B, signals of typical orthorhombic CoP (JCPDS: 29–0497) can be detected at the same time [32], confirming the successful formation of the Co_3B-CoP composite (Fig. 2b). After the reduction of Ru species on the Co_3B-CoP surface, new peaks appeared at 40.7 °, and 69.7 ° were attributed to the (111) and (220) crystal planes of Ru (JCPDS: 88–2333), indicating that Ru was successfully formed [33]. Furthermore, Figs. S2a-b showed that the as-prepared $Co(OH)_2$ and CoP are consistent with the corresponding standard spectra, and Ru signals

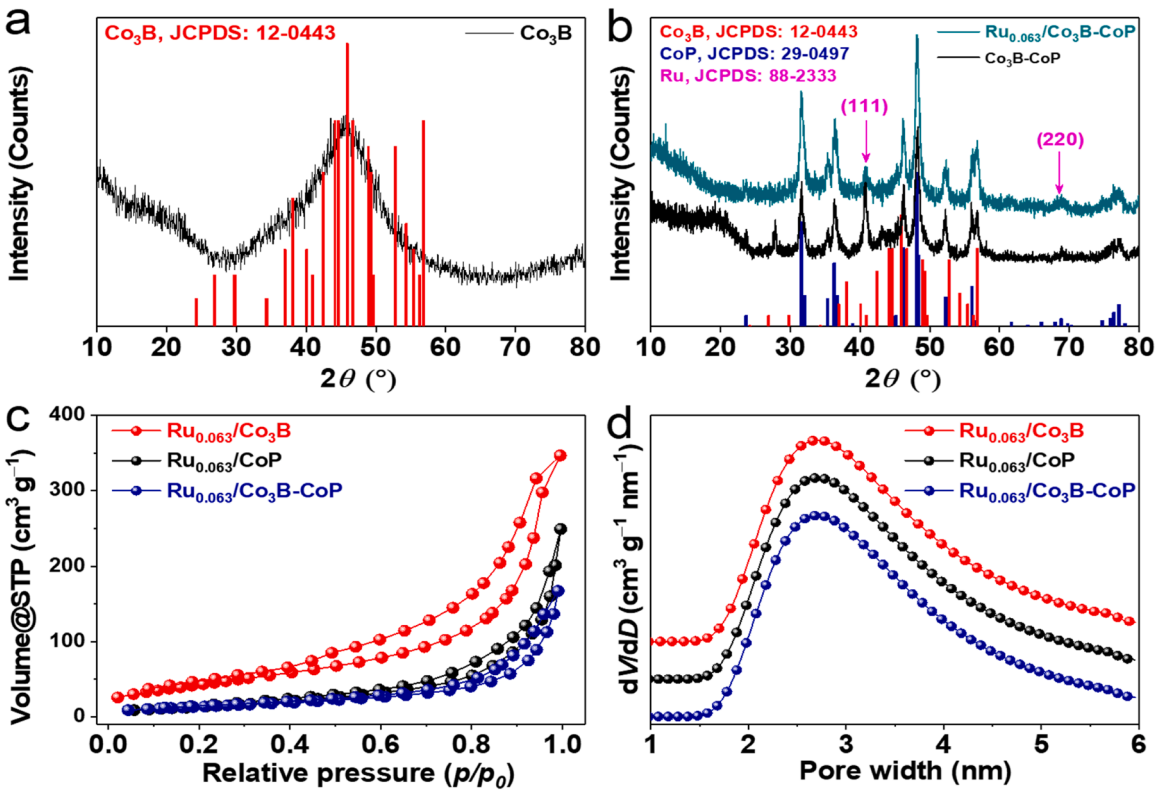

Fig. 2. XRD patterns of (a) Co_3B, (b) Co_3B-CoP and $Ru_{0.063}/Co_3B$-CoP. (c) N_2 adsorption–desorption isotherms and (d) the corresponding pore size distribution curves of $Ru_{0.063}/Co_3B$, $Ru_{0.063}$/CoP and $Ru_{0.063}/Co_3B$-CoP.

were also detected in $Ru_{0.063}$/CoP composite (Fig. S2c).

As presents in Fig. 2c, the textural features of the samples are investigated by N_2 adsorption-desorption isotherm. It exhibits a type III isotherm with typical hysteresis loop, indicating that the materials have the characteristics of mesoporous structure [34]. The Brunauer–Emmett–Teller (BET) surface areas of the $Ru_{0.063}/Co_3B$, $Ru_{0.063}$/CoP and $Ru_{0.063}/Co_3B$-CoP are 161.0, 54.8 and 50.4 $m^2\ g^{-1}$, respectively. Notably, the corresponding pore size distribution curves of all catalysts are similar, and the pore size is about 2.6 nm (Fig. 2d), which is mainly caused by the cracks and porous structures in the composite [35]. Besides, the specific surface areas of Co_3B, CoP and Co_3B-CoP are 49.0, 7.1 and 9.9 $m^2\ g^{-1}$, respectively (Fig. S3), indicating

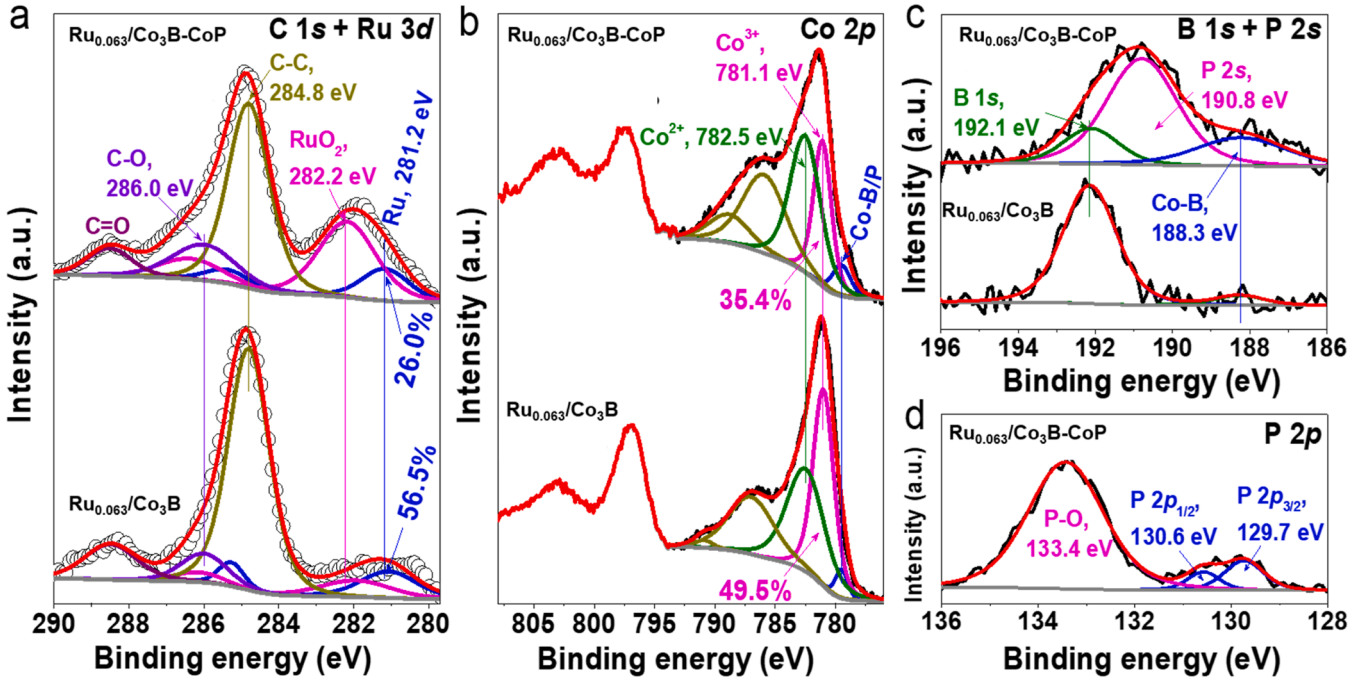

Fig. 3. High-resolution XPS spectra of (a) C 1*s* + Ru 3*d*, (b) Co 2*p*, (c) B 1*s* + P 2*s*, (d) P 2*p* regions of $Ru_{0.063}/Co_3B$ and/or $Ru_{0.063}/Co_3B$-CoP.

CoP blocked some of the surface areas of the Co_3B. Similar findings are reported in the literature [36,37]. The higher surface area exposes more active size; meanwhile, the high porosity helps the gas to diffuse along the surface. Moreover, nano-level dispersion of the conductive Ru particles enhances surface conductivity, which is suggested by lower resistance. The synergistic interaction between different components plays a more critical role in improving catalytic activity.

3.3. XPS analysis

The elemental composition and chemical state of the catalyst are further elucidated by X-ray photoelectron spectroscopy (XPS). XPS analysis of the catalysts confirm coexistence of C, O, B, P, Co and Ru elements (Fig. S4). The high-resolution XPS spectra of C 1*s* + Ru 3*d* regions are convoluted into two strong peaks at C–C (284.8 eV) and C–O (286.0 eV) and regard as calibration standard [38], while the binding energies at 281.2 and 282.2 eV are in turn corresponding to $3d_{5/2}$ of Ru metal and RuO_2 (Fig. 3a) [39,40]. The XPS results demonstrate chemical reduction of metallic Ru with 26.0% atomic percentage on the surface of Co_3B-CoP, which are much lower than that of Co_3B (56.5%), indicating that the surface characteristics of the composite can effectively adjust the chemical state of attachments. The oxidation reaction is unavoidable upon exposure to the air since the particle size of the Ru is very small and has a high surface area, which makes it easily oxidized. A similar observation on Ru-WO_3 and RuNi/CQDs was reported in the literature [41,42]. Since the oxidation of the Ru catalyst occurs only on the surface and the RuO_2 is reduced back to Ru during the $NaBH_4$ hydrolysis, the oxidation does not affect the performance. To be consistent with the literature reports [43,44], the $Ru_{0.063}/Co_3B$-CoP was used. Similar examples of reduced metallic Ru content and increased RuO_2 content were also observed for P-vacancy-rich CoP surfaces in our previous study [45].

As shown in Fig. 3b, the high-resolution Co 2*p* XPS spectra of $Ru_{0.063}/Co_3B$-CoP and $Ru_{0.063}/Co_3B$ are deconvoluted into Co-B/P (779.5 eV), Co^{3+} (781.1 eV), Co^{2+} (782.5 eV) and two satellite peaks, respectively [16]. The results indicate that the Co^{3+} content in $Ru_{0.063}/Co_3B$-CoP is 35.4%, which is much lower than that in $Ru_{0.063}/Co_3B$ (49.5%). This significant change in the chemical states of Ru and Co oxide species reflects the strong electronic interaction between them, which is speculated to be a key factor in improving the catalytic hydrolysis performance. Additionally, the high-resolution B 1*s* + P 2*s* further confirms the formation of Co-B alloy (B 1*s* of Co-B at 188.3 eV) in the two materials (Fig. 3c) [25,46]. The high-resolution P 2*p* indicates that there are abundant CoP components (P 2*p* of Co-P at 129.7 eV for $2p_{3/2}$ and 130.6 eV for $2p_{1/2}$) in the $Ru_{0.063}/Co_3B$-CoP composite (Fig. 3d) [47].

3.4. Catalytic hydrolysis analysis

The performance test of the catalyst is usually carried out in the solution of 150 mM $NaBH_4$ (containing 0.4 wt% NaOH) at 25 °C, and the schematic diagram of reaction device is shown in Fig. S5. In previous studies, we have found that the weak self-decomposition reaction occurs in the $NaBH_4$ aqueous solution (Fig. S6), and the extremely small HGR cannot meet people's needs. Considering that $NaBH_4$ can exist stably in alkaline solution (Fig. S7), we can produce H_2 on demand using catalysts. Here, a series of Ru-modified Co_3B-CoP catalysts were used to investigate the effect on the hydrolysis of $NaBH_4$. The mass percentage content of Ru particles in different catalysts is determined by ICP-AES (Table S2), which are 2.0, 4.7, 6.3, 8.9 and 11.3 wt%, respectively. As shown in Fig. 4a, the HGR presents a parabolic form with the increase of Ru species content, and when the loading is 6.3 wt%, it has the highest HGR value. Fig. 4b reveals that the optimal $Ru_{0.063}/Co_3B$-CoP catalyst possesses a HGR value reaching up to 8875.8 mL min^{-1} g_{cat}^{-1}, and the TOF is 636.0 mol min^{-1} mol_{Ru}^{-1}, outperforming most documented

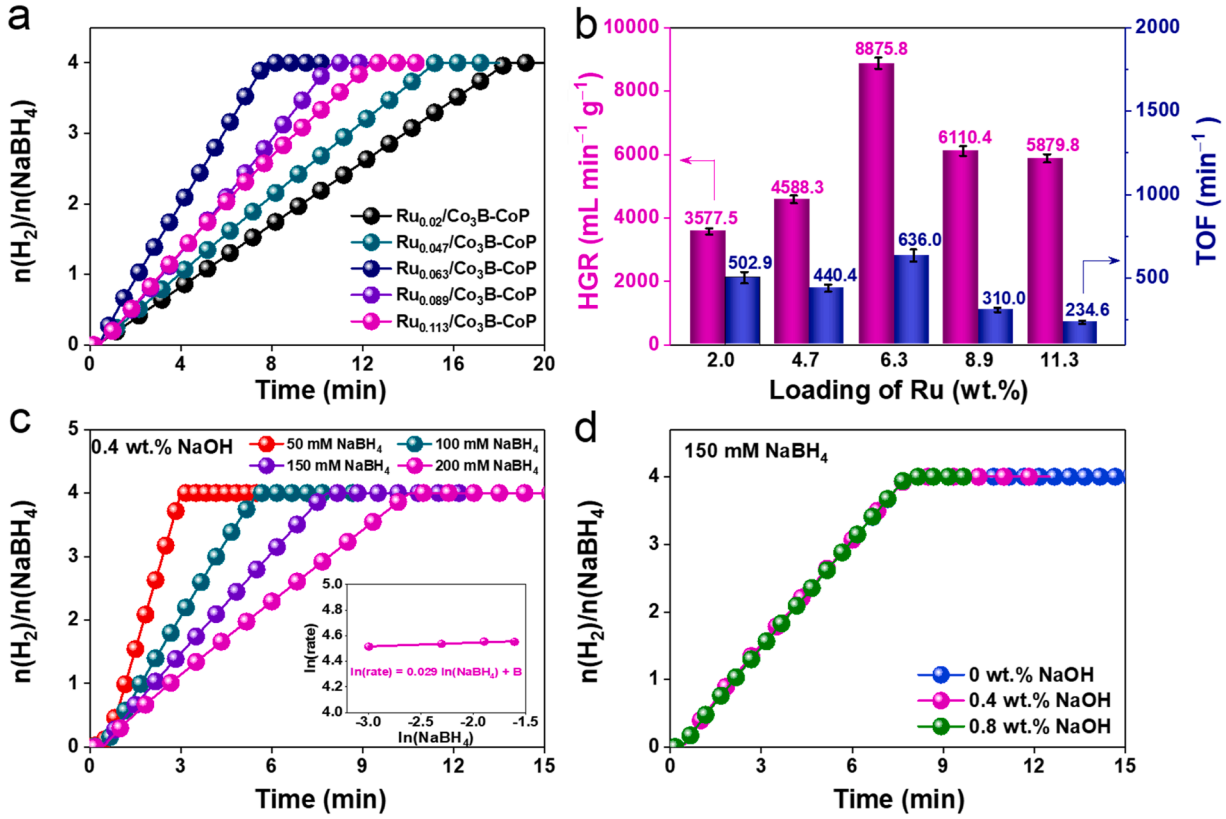

Fig. 4. Effect of catalytic $NaBH_4$ hydrolysis for H_2 generation under different conditions. (a) Different amounts of Ru. (b) The summarized TOF and HGR values. (c) The influence of $NaBH_4$ content on HGR at 0.4 wt% NaOH concentration (Inset: the corresponding plot of ln (rate) vs ln (concentration of $NaBH_4$)). (d) The influence of NaOH content on HGR with $NaBH_4$ concentration for 150 mM. All tests are performed at 298 K.

catalysts (Table S3). The high-efficiency catalytic performance can be attributed to the strong interaction between the different components in the $Ru_{0.063}/Co_3B$-CoP catalyst, and the suitable Ru content can form more grain boundaries, thereby exposing more active sites [48,49].

In order to explore the effect of $NaBH_4$ concentration on catalytic H_2 production, we kept NaOH concentration constant under different $NaBH_4$ concentrations. As shown in Fig. 4c, the HGR value remained almost constant with increasing $NaBH_4$ concentration in the 50–200 mM range. The relationship between ln (rate) and ln (concentration of $NaBH_4$) is fitted in the inset of Fig. 4c, and the slope value obtained corresponds to 0.029, which is close to zero. The results suggested that the hydrolysis reaction of $NaBH_4$ was a zero-level reaction, independent of the concentration of $NaBH_4$ [50]. Meanwhile, the effect of alkalinity on catalytic hydrolysis performance of $NaBH_4$ is also explored. In Fig. 4d, when the $NaBH_4$ concentration is fixed at 150 mM, the corresponding HGR is almost unaffected as the NaOH content changes. The effect of NaOH concentration on the HGR of $Ru_{0.063}/Co_3B$-CoP catalyst is consistent with the report by Wei et al. [51]. However, Yao et al. reported that the HGR of $NaBH_4$ hydrolysis was positively correlated with NaOH concentration in a specific concentration range; nevertheless, the HGR would decrease with a further increase in NaOH concentration [52]. These results suggest that the influence of NaOH concentration on $NaBH_4$ hydrolysis largely depends on the composition of the catalyst [53]. The kinetic studies revealed that the $NaBH_4$ hydrolysis follows "zero" order kinetics, and OH^- is one of the reactants [54]. Therefore, in theory, NaOH concentration should not affect the H_2 generation rate. Based on the above results, 150 mM $NaBH_4$ concentration and 0.4 wt% NaOH are selected as the solution for the study.

The factors affecting the hydrolysis of $NaBH_4$ for H_2 production are further analyzed using a series of comparative samples. As shown in Fig. 5a-b, Co_3B, CoP and Co_3B-CoP catalysts have lower HGR values for catalyzing $NaBH_4$ hydrolysis. Surprisingly, after loading the same amount of Ru on the above-mentioned substrates, the catalytic performances of Co_3B, CoP and Co_3B-CoP were enhanced by 2.01, 2.87 and 8.47 times, respectively, among which the $Ru_{0.063}/Co_3B$-CoP catalyst exhibits a maximum HGR value of 8875.8 mL_{H2} min^{-1} g_{cat}^{-1}. Fig. 5b shows that the HGR values of Co_3B and CoP are very close, even though the surface areas are different. This suggests the specific surface area is not a significant factor in determining the performance in this particular case. Moreover, combined with the poor performance of a single Ru catalyst (3012.2 mL_{H2} min^{-1} g_{cat}^{-1}, Fig. S8), the excellent catalytic $NaBH_4$ hydrolysis performance of $Ru_{0.063}/Co_3B$-CoP is attributed to the synergy between the Co_3B-CoP and Ru particles [55]. In this study, the novelty can be summarized as a scalable process, low-cost noble metal-based catalyst, and outstanding efficiency [56–58]. To analyze the activation energy of the catalyst, HGR is tested at different temperatures from 298 to 318 K. As shown in Fig. S9 and Fig. 5c, the HGR of Co_3B-CoP and $Ru_{0.063}/Co_3B$-CoP catalysts enhance rapidly with increasing temperature. The activation energy of the $Ru_{0.063}/Co_3B$-CoP catalyst is 47.6 kJ mol^{-1}, which is lower than that of the Co_3B-CoP catalyst (Fig. 5d) and many previously reported catalysts but not the lowest (Table S3). The low activation energy implies that the $Ru_{0.063}/Co_3B$-CoP catalyst has a lower energy barrier, thereby has a faster reaction kinetics during the reaction process [59].

Reusability is a crucial indicator for evaluating the performance of a catalyst, which is assessed through a continuous circulation test in 150 mM $NaBH_4$ (containing 0.4 wt% NaOH) solution. After each cycle of testing, we collect and vacuum dry the samples by centrifugation, and then add fresh $NaBH_4$ solution to continue the test. Fig. 5e-f exhibit the HGR and TOF values of $Ru_{0.063}/Co_3B$-CoP catalyst after five cycles, where the TOF value decreases from 645.5 to 443.9 min^{-1}. Owing to the catalyst loss during catalyst recovery and Ru leaching, the catalytic rate reduces to 68.8% of the original. The morphology (Fig. S10) and crystal structure (Fig. S11) of the $Ru_{0.063}/Co_3B$-CoP are slightly changed. Meanwhile, the TEM image of the $Ru_{0.063}/Co_3B$-CoP catalyst after five cycles of stability tests shows that the average particle size of Ru nanoparticles is 1.68 nm (Fig. S12). The high-resolution XPS spectra of Ru 3*d* and Co 2*p* prove that the chemical states of the elements have changed significantly; for example, the content of Ru metal and Co^{3+} increase markedly after five cycles (Fig. S13). The increase in the Ru metal content could be due to the robust reduction environment, and the growing Co^{3+} content could indicate the Co_3B leaching. The analysis suggests that the change of surface chemical states mainly cause the continuous decrease in catalytic performance, the exfoliation of Ru

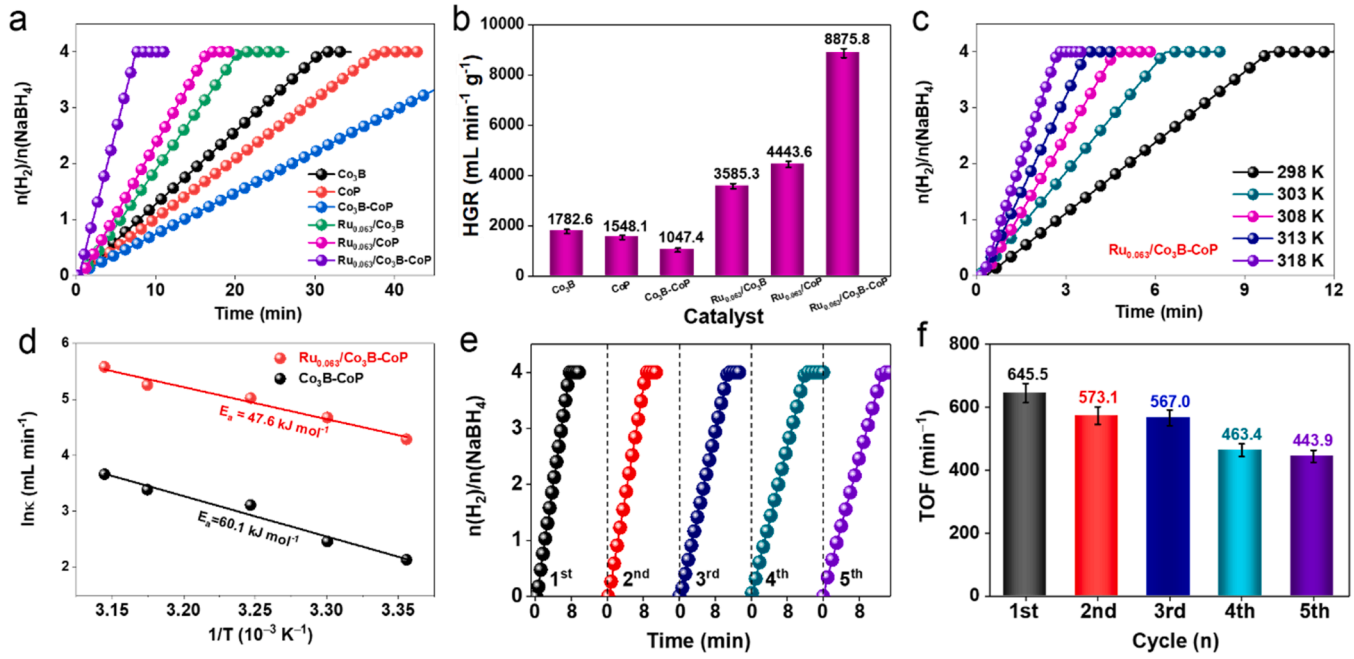

Fig. 5. (a) The relationship between the H_2 generation rates and reaction time of different catalysts, and (b) the summarized HGR values. (c) The relationship between catalytic $NaBH_4$ hydrolysis temperature and HGR in the range of 298–318 K. (d) The summarized Arrhenius diagram of $Ru_{0.063}/Co_3B$-CoP and Co_3B-CoP. (e) Cycle stability test of $Ru_{0.063}/Co_3B$-CoP catalyst. (f) The summarized TOF values from e. All tests are performed in 150 mM $NaBH_4$ + 0.4 wt% NaOH solution.

particles (Table S2) and BO_2^- poisoning [60].

3.5. DFT calculations

DFT calculation is conducted to understand the superior catalytic hydrolysis performance. Systematic studies have demonstrated that half of the hydrogens produced by the $NaBH_4$ hydrolysis come from water, which is favourable to improving hydrogen yield (Eq. 1) [61]. As shown in Fig. 6a, the deformed charge density of the heterostructure presents a significant charge accumulation at the interface of two materials, confirming the strong synergistic effect between Ru and Co_3B-CoP. Subsequently, we investigate the Bader charges of Ru atoms on $Ru_{0.063}$/CoP, $Ru_{0.063}$/Co_3B and $Ru_{0.063}$/Co_3B-CoP catalysts, and the charges adsorbed on Ru are − 0.0045 e, − 0.0359 e and − 0.0604 e (Fig. 6b), respectively. Meanwhile, the charge distribution of the adsorbed BH_4^- ions indicates that the B ions are positively charged (Fig. S14). The results indicate that the electrons around Ru are enriched; thereby, BH_4^- groups are more inclined to adsorb on the Ru site due to the partially positively charged B atom. Fig. S15 displays the schematic diagram of hydrogen production of $Ru_{0.063}$/CoP, $Ru_{0.063}$/Co_3B and $Ru_{0.063}$/Co_3B-CoP catalysts. The adsorption energies of BH_4^* + H_2O^* on the surfaces of $Ru_{0.063}$/CoP, $Ru_{0.063}$/Co_3B and $Ru_{0.063}$/Co_3B-CoP catalysts are − 4.17, − 3.98 and − 4.24 eV, respectively, indicating that BH_4^* + H_2O^* species are adsorbed readily to the surface of Ru particles in $Ru_{0.063}$/Co_3B-CoP (Fig. 6c). Meanwhile, comparing with $Ru_{0.063}$/CoP (ΔG_3 =1.38 eV) and $Ru_{0.063}$/Co_3B (ΔG_3 =2.67 eV), the optimized $Ru_{0.063}$/Co_3B-CoP (ΔG_3 =1.12 eV) exhibits the lowest energy barrier, implying the highest hydrogen production activity (Table S1).

3.6. Catalytic mechanism analysis

As discussed above, the designed $Ru_{0.063}$/Co_3B-CoP catalyst exhibits good catalytic activity, which is mainly related to the composition of hybrid materials and the strong interaction between different components. As shown in Fig. 6d, a possible reaction mechanism based on Langmuir-Hinshelwood model has been proposed to catalyze the hydrolysis of $NaBH_4$ for H_2 generation [62]. Initially, the dissolved BH_4^- ions are selectively adsorbed on the surface of the Ru particles due to the abundant vacant 4*d* orbitals on Ru atoms [63]. This result is consistent with the transfer of electrons from CoP to Ru species caused by the work function (Ru: 4.71 eV, RuO_2: 5.0 eV, CoP: 4.227 eV and CoB alloy) [45, 64], making the electron-rich Ru site to adsorb B atoms with a little positive charge in BH_4^- ions. DFT calculations further demonstrate that the Co_3B-CoP composite can donate more electrons to Ru particles

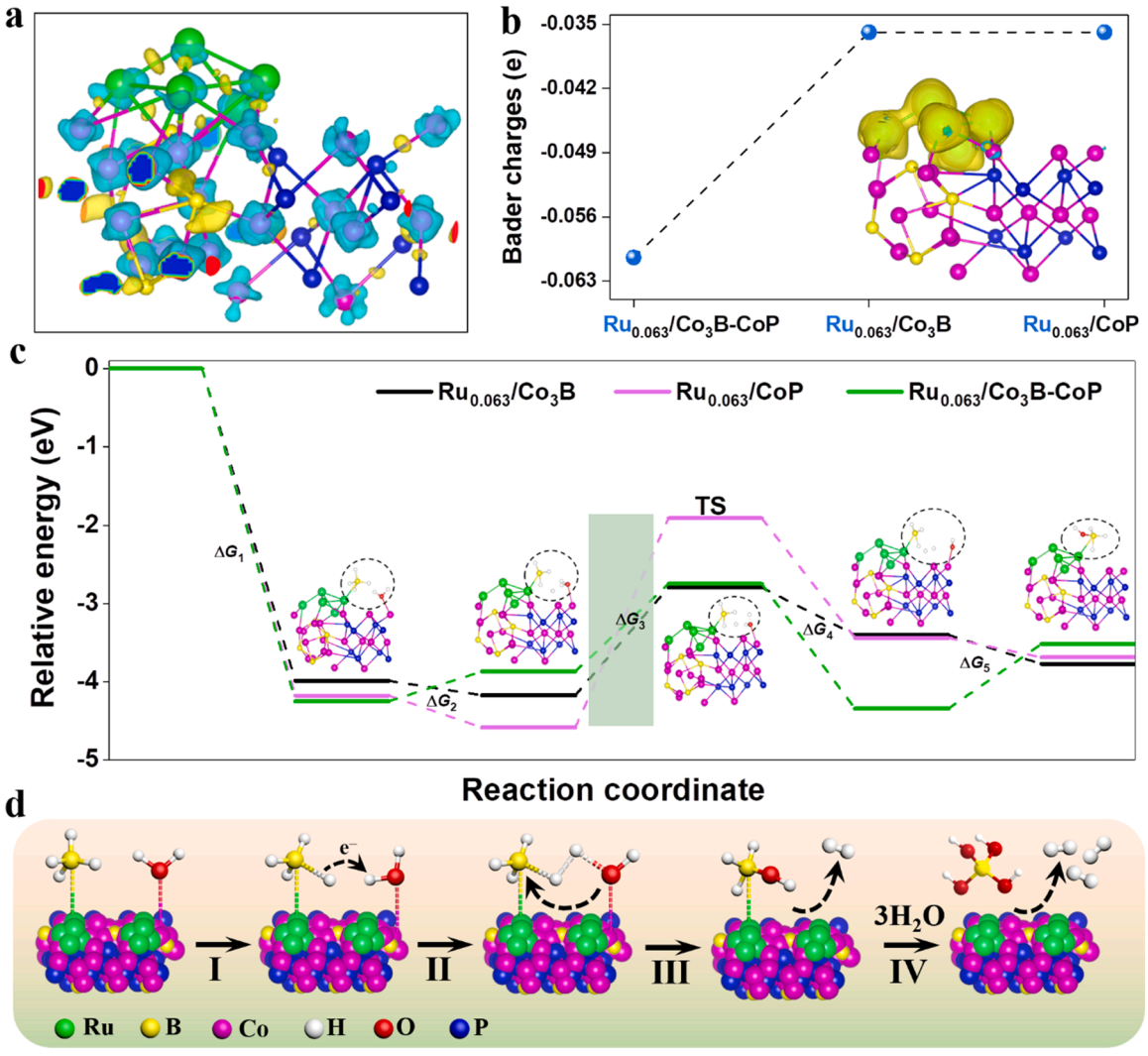

Fig. 6. (a) Schematic diagram of the deformed charge density distribution of catalyst $Ru_{0.063}$/Co_3B-CoP catalyst. The blue, pink, yellow, and green balls represent P, Co, B, and Ru atoms, respectively. (b) Bader charges of Ru atoms on $Ru_{0.063}$/CoP, $Ru_{0.063}$/Co_3B and $Ru_{0.063}$/Co_3B-CoP catalysts. (c) The free energy curves of $Ru_{0.063}$/CoP, $Ru_{0.063}$/Co_3B and $Ru_{0.063}$/Co_3B-CoP for the hydrolysis of sodium borohydride. (d) Catalytic mechanism diagram of H_2 production by hydrolysis of $NaBH_4$ based on $Ru_{0.063}$/Co_3B-CoP catalyst.

compared with single CoP and Co_3B, and the electron-rich Ru particles are beneficial for BH_4^- adsorption and H_2 desorption during the catalytic hydrolysis process. Meanwhile, the electron-deficient binary Co_3B-CoP sites can adsorb abundant water molecules. At the interface, the adsorbed H_2O molecules can attack BH_4^- ions to release a H_2 molecule and form a BH_3OH^- intermediate [65]. As the reaction proceeds, the remaining H atoms in the borohydride are replaced by OH^- ions, which are eventually decomposed into $B(OH)_4^-$ species [66].

4. Conclusions

In summary, the $Ru_{0.063}/Co_3B$-CoP heterostructure is successfully fabricated by chemical deposition and vapor phase phosphating process. Various characterization techniques, such as XRD, SEM, TEM, BET and XPS, have explored the crystal structure, morphology, porosity and chemical state of the material. The resulted $Ru_{0.063}/Co_3B$-CoP catalyst shows excellent catalytic activity in catalyzing the hydrolysis of $NaBH_4$ for H_2 generation. Based on various characterizations and reaction processes, a reliable catalytic mechanism is proposed. The analysis suggests that the change of the surface chemical state caused by the strong interaction between the components in the $Ru_{0.063}/Co_3B$-CoP catalyst is the key to improving the H_2 generation during the catalytic $NaBH_4$ hydrolysis process. This work has important theoretical and practical significance for the development of novel and efficient catalysts for H_2 production from $NaBH_4$ hydrolysis.

CRediT authorship contribution statement

Shuqing Zhou: Writing – original draft, Methodology. **Lianrui Cheng:** Data curation. **Yi Huang:** Investigation. **Yi Liu:** Methodology. **Luyan Shi** : Data curation, Investigation. **Tayirjan Taylor Isimjan:** Writing – review & editing. **Xiulin Yang:** Writing – review & editing, Supervision.

Declaration of Competing Interest

The authors declare that they have no known competing financial interests or personal relationships that could have appeared to influence the work reported in this paper.

Data Availability

The data that has been used is confidential.

Acknowledgements

This work has been supported by the National Natural Science Foundation of China (no. 21965005), Natural Science Foundation of Guangxi Province (2021GXNSFAA076001), Research Program of Young Teachers in Universities of Guangxi (2022KY0047), Project of High-Level Talents of Guangxi (F-KA18015) and Guangxi Technology Base and Talent Subject (GUIKE AD18126001, GUIKE AD20297039).

Appendix A. Supporting information

Supplementary data associated with this article can be found in the online version at doi:10.1016/j.apcatb.2023.122519.

References

[1] J. Deng, S. Chen, N. Yao, Q. Wang, J. Li, Z. Wei, Integrating H_2 generation with sewage disposal by an efficient anti-poisoning bifunctional electrocatalyst, Appl. Catal. B Environ. 277 (2020), 119175, https://doi.org/10.1016/j.apcatb.2020.119175.

[2] A. Magnuson, F. Mamedov, J. Messinger, Toward sustainable H_2 production: linking hydrogenase with photosynthesis, Joule 4 (2020) 1157–1159, https://doi.org/10.1016/j.joule.2020.05.014.

[3] S. Özkar, M. Zahmakıran, Hydrogen generation from hydrolysis of sodium borohydride using Ru(0) nanoclusters as catalyst, J. Alloy. Compd. 404–406 (2005) 728–731, https://doi.org/10.1016/j.jallcom.2004.10.084.

[4] P. Gabrielli, A. Poluzzi, G.J. Kramer, C. Spiers, M. Mazzotti, M. Gazzani, Seasonal energy storage for zero-emissions multi-energy systems via underground hydrogen storage, Renew. Sustain Energy Rev. 121 (2020), 109629, https://doi.org/10.1016/j.rser.2019.109629.

[5] J. Zhu, L. Hu, P. Zhao, L.Y.S. Lee, K.-Y. Wong, Recent advances in electrocatalytic hydrogen evolution using nanoparticles, Chem. Rev. 120 (2020) 851–918, https://doi.org/10.1021/acs.chemrev.9b00248.

[6] Z. Ma, S. Panda, Q. Zhang, F. Sun, D. Khan, W. Ding, J. Zou, Improving hydrogen sorption performances of MgH_2 through nanoconfinement in a mesoporous CoS nano-boxes scaffold, Chem. Eng. J. 406 (2021), 126790, https://doi.org/10.1016/j.cej.2020.126790.

[7] X. Liu, G.S. McGrady, H.W. Langmi, C.M. Jensen, Facile cycling of Ti-doped $LiAlH_4$ for high performance hydrogen storage, J. Am. Chem. Soc. 131 (2009) 5032–5033, https://doi.org/10.1021/ja809917g.

[8] X. Zhang, Q. Zhang, B. Xu, X. Liu, K. Zhang, G. Fan, W. Jiang, Efficient hydrogen generation from the $NaBH_4$ hydrolysis by cobalt-based catalysts: positive roles of sulfur-containing salts, ACS Appl. Mater. Interfaces 12 (2020) 9376–9386, https://doi.org/10.1021/acsami.9b22645.

[9] J. Guo, B. Wang, D. Yang, Z. Wan, P. Yan, J. Tian, T.T. Isimjan, X. Yang, Rugae-like Ni_2P-CoP nanoarrays as a bi-functional catalyst for hydrogen generation: $NaBH_4$ hydrolysis and water reduction, Appl. Catal. B Environ. 265 (2020), 118584, https://doi.org/10.1016/j.apcatb.2019.118584.

[10] M. Masjedi, L.T. Yildirim, S. Özkar, Novel homogeneous catalyst comprising ruthenium and trimethylphosphite for the hydrolysis of sodium borohydride, J. Mol. Catal. A Chem. 355 (2012) 186–191, https://doi.org/10.1016/j.molcata.2011.12.015.

[11] Y. Zhu, L. Ouyang, H. Zhong, J. Liu, H. Wang, H. Shao, Z. Huang, M. Zhu, Closing the loop for hydrogen storage: facile regeneration of $NaBH_4$ from its hydrolytic product, Angew. Chem. Int. Ed. 59 (2020) 8623–8629, https://doi.org/10.1002/anie.201915988.

[12] Ç. Çakanyıldırım, M. Gürü, Decomposition of $NaBH_4$ with self-regeneration of carbon-supported $CoCl_2$ catalyst, Int. J. Hydrog. Energy 14 (2017) 1005–1010, https://doi.org/10.1080/15435075.2017.1354297.

[13] M. Zahmakıran, S. Özkar, Water dispersible acetate stabilized ruthenium(0) nanoclusters as catalyst for hydrogen generation from the hydrolysis of sodium borohyride, J. Mol. Catal. A Chem. 258 (2006) 95–103, https://doi.org/10.1016/j.molcata.2006.05.037.

[14] M. Zahmakiran, S. Özkar, Intrazeolite ruthenium(0) nanoclusters: a superb catalyst for the hydrogenation of benzene and the hydrolysis of sodium borohydride, Langmuir 24 (2008) 7065–7067, https://doi.org/10.1021/la800874u.

[15] H. Zhong, L. Ouyang, M. Zeng, J. Liu, H. Wang, H. Shao, M. Felderhoff, M. Zhu, Realizing facile regeneration of spent $NaBH_4$ with Mg–Al alloy, J. Mater. Chem. A 7 (2019) 10723–10728, https://doi.org/10.1039/c9ta00769e.

[16] J. Guo, C. Wu, J. Zhang, P. Yan, J. Tian, X. Shen, T.T. Isimjan, X. Yang, Hierarchically structured rugae-like RuP_3–CoP arrays as robust catalysts synergistically promoting hydrogen generation, J. Mater. Chem. A 7 (2019) 8865–8872, https://doi.org/10.1039/c8ta10695a.

[17] L. Kong, T. Yu, J. Zhan, Y. Zhang, G. Li, H. Wang, X. Wang, L. Cheng, F. Wang, Study on the performance of $NaBH_4$ using Ru-Co/CNTs catalyst to catalyze alcoholysis to produce hydrogen, Fuller. Nanotub. Carbon Nanostruct. 28 (2020) 891–899, https://doi.org/10.1080/1536383x.2020.1777544.

[18] Y.M. Zhang, J. Zou, Y.M. Luo, F.H. Wang, Study on preparation and performance of Ru-Fe/GO catalyst for sodium borohydride alcoholysis to produce hydrogen, Fuller. Nanotub. Carbon Nanostruct. 28 (2020) 786–793, https://doi.org/10.1080/1536383x.2020.1760849.

[19] S. Akbayrak, Y. Tonbul, S. Özkar, Magnetically separable Rh^0/Co_3O_4 nanocatalyst provides over a million turnovers in hydrogen release from ammonia borane, ACS Sustain. Chem. Eng. 8 (2020) 4216–4224, https://doi.org/10.1021/acssuschemeng.9b07402.

[20] C. Wu, J. Zhang, J. Guo, L. Sun, J. Ming, H. Dong, Y. Zhao, J. Tian, X. Yang, Ceria-induced strategy to tailor Pt atomic clusters on cobalt–nickel oxide and the synergetic effect for superior hydrogen generation, ACS Sustain. Chem. Eng. 6 (2018) 7451–7457, https://doi.org/10.1021/acssuschemeng.8b00061.

[21] S. Akbayrak, M. Kaya, M. Volkan, S. Ozkar, Palladium(0) nanoparticles supported on silica-coated cobalt ferrite: a highly active, magnetically isolable and reusable catalyst for hydrolytic dehydrogenation of ammonia borane, Appl. Catal. B Environ. 147 (2014) 387–393, https://doi.org/10.1016/j.apcatb.2013.09.023.

[22] L. Chong, J. Wen, J. Kubal, F.G. Sen, J. Zou, J. Greeley, M. Chan, H. Barkholtz, W. Ding, D.-J. Liu, Ultralow-loading platinum-cobalt fuel cell catalysts derived from imidazolate frameworks, Science 362 (2018) 1276–1281, https://doi.org/10.1126/science.aau0630.

[23] H. Yuan, S. Wang, Z. Ma, M. Kundu, B. Tang, J. Li, X. Wang, Oxygen vacancies engineered self-supported B doped Co_3O_4 nanowires as an efficient multifunctional catalyst for electrochemical water splitting and hydrolysis of sodium borohydride, Chem. Eng. J. 404 (2021), 126474, https://doi.org/10.1016/j.cej.2020.126474.

[24] H. Zhang, G. Xu, L. Zhang, W. Wang, W. Miao, K. Chen, L. Cheng, Y. Li, S. Han, Ultrafine cobalt nanoparticles supported on carbon nanospheres for hydrolysis of sodium borohydride, Renew. Energy 162 (2020) 345–354, https://doi.org/10.1016/j.renene.2020.08.031.

[25] J. Masa, P. Weide, D. Peeters, I. Sinev, W. Xia, Z. Sun, C. Somsen, M. Muhler, W. Schuhmann, Amorphous cobalt boride (Co_2B) as a highly efficient nonprecious catalyst for electrochemical water splitting: oxygen and hydrogen evolution, Adv. Energy Mater. 6 (2016), 1502313, https://doi.org/10.1002/aenm.201502313.

[26] A. Zhang, J. Xia, Q. Yao, Z.-H. Lu, Pd–WO heterostructures immobilized by MOFs-derived carbon cage for formic acid dehydrogenation, Appl. Catal. B Environ. 309 (2022), 121278, https://doi.org/10.1016/j.apcatb.2022.121278.
[27] G. Meng, H. Tian, L. Peng, Z. Ma, Y. Chen, C. Chen, Z. Chang, X. Cui, J. Shi, Ru to W electron donation for boosted HER from acidic to alkaline on Ru/WNO sponges, Nano Energy 80 (2021), 105531, https://doi.org/10.1016/j.nanoen.2020.105531.
[28] S. Ye, W. Xiong, P. Liao, L. Zheng, X. Ren, C. He, Q. Zhang, J. Liu, Removing the barrier to water dissociation on single-atom Pt sites decorated with a CoP mesoporous nanosheet array to achieve improved hydrogen evolution, J. Mater. Chem. A 8 (2020) 11246–11254, https://doi.org/10.1039/d0ta02936j.
[29] A.M. Zieschang, J.D. Bocarsly, J. Schuch, C.V. Reichel, B. Kaiser, W. Jaegermann, R. Seshadri, B. Albert, Magnetic and electrocatalytic properties of nanoscale cobalt boride, Co_3B, Inorg. Chem. 58 (2019) 16609–16617, https://doi.org/10.1021/acs.inorgchem.9b02617.
[30] Y. Qian, F. Zhang, H. Pang, A review of MOFs and their composites-based photocatalysts: synthesis and applications, Adv. Funct. Mater. 31 (2021), 2104231, https://doi.org/10.1002/adfm.202104231.
[31] L. Shi, P. Wang, Q. Wang, X. Ren, F. Ichihara, W. Zhou, H. Zhang, Y. Izumi, B. Cao, S. Wang, H. Chen, J. Ye, Efficient photocatalytic CO_2 reduction mediated by transitional metal borides: metal site-dependent activity and selectivity, J. Mater. Chem. A 8 (2020) 21833–21841, https://doi.org/10.1039/d0ta07072f.
[32] J. Liu, Y. Gao, X. Tang, K. Zhan, B. Zhao, B.Y. Xia, Y. Yan, Metal–organic framework-derived hierarchical ultrathin CoP nanosheets for overall water splitting, J. Mater. Chem. A 8 (2020) 19254–19261, https://doi.org/10.1039/d0ta07616c.
[33] Y. Wang, M. Zheng, H. Sun, X. Zhang, C. Luan, Y. Li, L. Zhao, H. Zhao, X. Dai, J.-Y. Ye, H. Wang, S.-G. Sun, Catalytic Ru containing Pt_3Mn nanocrystals enclosed with high-indexed facets: Surface alloyed Ru makes Pt more active than Ru particles for ethylene glycol oxidation, Appl. Catal. B Environ. 253 (2019) 11–20, https://doi.org/10.1016/j.apcatb.2019.04.022.
[34] S. Dou, S. Zhou, H. Huang, P. Yan, E. Shoko, T.T. Isimjan, X. Yang, Metal–organic framework (MOF)-derived electron-transfer enhanced homogeneous PdO-Rich Co_3O_4 as a highly efficient bifunctional catalyst for sodium borohydride hydrolysis and 4-nitrophenol reduction, Chem. Eur. J. 26 (2020) 16923–16931, https://doi.org/10.1002/chem.202003793.
[35] Q.M. Peng, Q.T. He, Y. Hu, T.T. Isimjan, R.B. Hou, X.L. Yang, Interface engineering of porous Fe_2P-$WO_{2.92}$ catalyst with oxygen vacancies for highly active and stable large-current oxygen evolution and overall water splitting, J. Energy Chem. 65 (2022) 574–582, https://doi.org/10.1016/j.jechem.2021.06.037.
[36] J. Li, X. Hong, Y. Wang, Y. Luo, P. Huang, B. Li, K. Zhang, Y. Zou, L. Sun, F. Xu, F. Rosei, S.P. Verevkin, A.A. Pimerzin, Encapsulated cobalt nanoparticles as a recoverable catalyst for the hydrolysis of sodium borohydride, Energy Storage Mater. 27 (2020) 187–197, https://doi.org/10.1016/j.ensm.2020.01.011.
[37] H.X. Wang, Y.W. Wang, L.X. Tan, L. Fang, X.H. Yang, Z.Y. Huang, J. Li, H.J. Zhang, Y. Wang, Component-controllable cobalt telluride nanoparticles encapsulated in nitrogen-doped carbon frameworks for efficient hydrogen evolution in alkaline conditions, Appl. Catal. B Environ. 244 (2019) 568–575, https://doi.org/10.1016/j.apcatb.2018.11.081.
[38] Z. Wan, D. Yang, J. Chen, J. Tian, T.T. Isimjan, X. Yang, Oxygen-evolution catalysts based on iron-mediated nickel metal–organic frameworks, ACS Appl. Nano Mater. 2 (2019) 6334–6342, https://doi.org/10.1021/acsanm.9b01330.
[39] X. Cui, P. Ren, C. Ma, J. Zhao, R. Chen, S. Chen, N.P. Rajan, H. Li, L. Yu, Z. Tian, D. Deng, Robust interface Ru centers for high-performance acidic oxygen evolution, Adv. Mater. 32 (2020), 1908126, https://doi.org/10.1002/adma.201908126.
[40] M. Zahmakiran, S. Özkar, Zeolite-confined ruthenium(0) nanoclusters catalyst: record catalytic activity, reusability, and lifetime in hydrogen generation from the hydrolysis of sodium borohydride, Langmuir 25 (2009) 2667–2678, https://doi.org/10.1021/la803391c.
[41] C. Rajkumar, B. Thirumalraj, S.-M. Chen, P. Veerakumar, S.-B. Liu, Ruthenium nanoparticles decorated tungsten oxide as a bifunctional catalyst for electrocatalytic and catalytic applications, ACS Appl. Mater. Interfaces 9 (2017) 31794–31805, https://doi.org/10.1021/acsami.7b07645.
[42] Y. Liu, X. Li, Q. Zhang, W. Li, Y. Xie, H. Liu, L. Shang, Z. Liu, Z. Chen, L. Gu, Z. Tang, T. Zhang, S. Lu, A general route to prepare low-ruthenium-content bimetallic electrocatalysts for pH-universal hydrogen evolution reaction by using carbon quantum dots, Angew. Chem. Int. Ed. 59 (2020) 1718–1726, https://doi.org/10.1002/anie.201913910.
[43] R. Jiang, Y. Da, J. Zhang, H. Wu, B. Fan, J. Li, J. Wang, Y. Deng, X. Han, W. Hu, Non-equilibrium synthesis of stacking faults-abundant Ru nanoparticles towards electrocatalytic water splitting, Appl. Catal. B Environ. 316 (2022), 121682, https://doi.org/10.1016/j.apcatb.2022.121682.
[44] D. Li, R. Li, M. Lu, X. Lin, Y. Zhan, L. Jiang, Carbon dioxide reforming of methane over Ru catalysts supported on Mg-Al oxides: a highly dispersed and stable Ru/Mg(Al)O catalyst, Appl. Catal. B Environ. 200 (2017) 566–577, https://doi.org/10.1016/j.apcatb.2016.07.050.
[45] S. Zhou, Y. Yang, W. Zhang, X. Rao, P. Yan, T.T. Isimjan, X. Yang, Structure-regulated Ru particles decorated P-vacancy-rich CoP as a highly active and durable catalyst for $NaBH_4$ hydrolysis, J. Colloid Interface Sci. 591 (2021) 221–228, https://doi.org/10.1016/j.jcis.2021.02.009.
[46] S. Gupta, M.K. Patel, A. Miotello, N. Patel, Metal boride-based catalysts for electrochemical water-splitting: a review, Adv. Funct. Mater. 30 (2019), 1906481, https://doi.org/10.1002/adfm.201906481.
[47] H. Qi, Y.-L. Lee, T. Yang, W. Li, W. Li, L. Ma, S. Hu, Y. Duan, G.A. Hackett, X. Liu, Positive effects of H_2O on the hydrogen oxidation reaction on $Sr_2Fe_{1.5}Mo_{0.5}O_{6-\delta}$-based perovskite anodes for solid oxide fuel cells, ACS Catal. 10 (2020) 5567–5578, https://doi.org/10.1021/acscatal.9b05458.
[48] D. Wang, Q. Li, C. Han, Z. Xing, X. Yang, Single-atom ruthenium based catalyst for enhanced hydrogen evolution, Appl. Catal. B Environ. 249 (2019) 91–97, https://doi.org/10.1016/j.apcatb.2019.02.059.
[49] M.R. Axet, K. Philippot, Catalysis with Colloidal Ruthenium Nanoparticles, Chem. Rev. 120 (2020) 1085–1145, https://doi.org/10.1021/acs.chemrev.9b00434.
[50] M. Masjedi, T. Demiralp, S. Özkar, Testing catalytic activity of ruthenium(III) acetylacetonate in the presence of trialkylphosphite or trialkylphosphine in hydrogen generation from the hydrolysis of sodium borohydride, J. Mol. Catal. A Chem. 310 (2009) 59–63, https://doi.org/10.1016/j.molcata.2009.05.022.
[51] R. Fernandes, N. Patel, A. Miotello, Hydrogen generation by hydrolysis of alkaline $NaBH_4$ solution with Cr-promoted Co–B amorphous catalyst, Appl. Catal. B Environ. 92 (2009) 68–74, https://doi.org/10.1016/j.apcatb.2009.07.019.
[52] L. Yao, X. Li, W. Peng, Q. Yao, J. Xia, Z.-H. Lu, Co-CeO_x nanoparticles anchored on a nitrogen-doped carbon nanosheet: a synergistic effect for highly efficient hydrolysis of sodium borohydride, Inorg. Chem. Front. 8 (2021) 1056–1065, https://doi.org/10.1039/d0qi01244k.
[53] S.U. Jeong, R.K. Kim, E.A. Cho, H.J. Kim, S.W. Nam, I.H. Oh, S.A. Hong, S.H. Kim, A study on hydrogen generation from $NaBH_4$ solution using the high-performance Co-B catalyst, J. Power Sources 144 (2005) 129–134, https://doi.org/10.1016/j.jpowsour.2004.12.046.
[54] Z. Liu, B. Guo, S.H. Chan, E.H. Tang, L. Hong, Pt and Ru dispersed on $LiCoO_2$ for hydrogen generation from sodium borohydride solutions, J. Power Sources 176 (2008) 306–311, https://doi.org/10.1016/j.jpowsour.2007.09.114.
[55] J. Yu, A. Wang, W. Yu, X. Liu, X. Li, H. Liu, Y. Hu, Y. Wu, W. Zhou, Tailoring the ruthenium reactive sites on N doped molybdenum carbide nanosheets via the anti-Ostwald ripening as efficient electrocatalyst for hydrogen evolution reaction in alkaline media, Appl. Catal. B Environ. 277 (2020), 119236, https://doi.org/10.1016/j.apcatb.2020.119236.
[56] N. Sahiner, Modified multi-wall carbon nanotubes as metal free catalyst for application in H_2 production from methanolysis of $NaBH_4$, J. Power Sources 366 (2017) 178–184, https://doi.org/10.1016/j.jpowsour.2017.09.041.
[57] C.-C. Chou, C.-H. Hsieh, B.-H. Chen, Hydrogen generation from catalytic hydrolysis of sodium borohydride using bimetallic Ni–Co nanoparticles on reduced graphene oxide as catalysts, Energy 90 (2015) 1973–1982, https://doi.org/10.1016/j.energy.2015.07.023.
[58] Ö. Şahin, D.E. Karakaş, M. Kaya, C. Saka, The effects of plasma treatment on electrochemical activity of Co–B–P catalyst for hydrogen production by hydrolysis of $NaBH_4$, J. Energy Inst. 90 (2017) 466–475, https://doi.org/10.1016/j.joei.2016.03.003.
[59] S. Dou, W. Zhang, Y. Yang, S. Zhou, X. Rao, P. Yan, T.T. Isimjan, X. Yang, Shaggy-like Ru-clusters decorated core-shell metal-organic framework-derived CoO_x@NPC as high-efficiency catalyst for $NaBH_4$ hydrolysis, Int. J. Hydrog. Energy 46 (2021) 7772–7781, https://doi.org/10.1016/j.ijhydene.2020.12.011.
[60] L.M. Zhou, J. Meng, P. Li, Z.L. Tao, L.Q. Mai, J. Chen, Ultrasmall cobalt nanoparticles supported on nitrogen-doped porous carbon nanowires for hydrogen evolution from ammonia borane, Mater. Horiz. 4 (2017) 268–273, https://doi.org/10.1039/c6mh00534a.
[61] H. Zhang, L. Zhang, I.A. Rodríguez-Pérez, W. Miao, K. Chen, W. Wang, Y. Li, S. Han, Carbon nanospheres supported bimetallic Pt-Co as an efficient catalyst for $NaBH_4$ hydrolysis, Appl. Surf. Sci. 540 (2021), 148296, https://doi.org/10.1016/j.apsusc.2020.148296.
[62] H.N. Abdelhamid, A review on hydrogen generation from the hydrolysis of sodium borohydride, Int. J. Hydrog. Energy 46 (2021) 726–765, https://doi.org/10.1016/j.ijhydene.2020.09.186.
[63] J. Jiang, S. Tao, Q. He, J. Wang, Y. Zhou, Z. Xie, W. Ding, Z. Wei, Interphase-oxidized ruthenium metal with half-filled d-orbitals for hydrogen oxidation in an alkaline solution, J. Mater. Chem. A 8 (2020) 10168–10174, https://doi.org/10.1039/D0TA02528C.
[64] H.K. Kim, I.-H. Yu, J.H. Lee, T.J. Park, C.S. Hwang, Scaling of equivalent oxide thickness of atomic layer deposited HfO_2 film using RuO_2 electrodes suppressing the dielectric dead-layer effect, Appl. Phys. Lett. 101 (2012), 172910, https://doi.org/10.1063/1.4764541.
[65] A.A. Kassem, H.N. Abdelhamid, D.M. Fouad, S.A. Ibrahim, Metal-organic frameworks (MOFs) and MOFs-derived CuO@C for hydrogen generation from sodium borohydride, Int. J. Hydrog. Energy 44 (2019) 31230–31238, https://doi.org/10.1016/j.ijhydene.2019.10.047.
[66] A.E. Genç, A. Akça, B. Kutlu, The catalytic effect of the Au(111) and Pt(111) surfaces to the sodium borohydride hydrolysis reaction mechanism: a DFT study, Int. J. Hydrog. Energy 43 (2018) 14347–14359, https://doi.org/10.1016/j.ijhydene.2018.06.026.